EFDA–JET–PR(12)06

Hyun-Tae Kim, W. Fundamenski, A.C.C. Sips
and JET EFDA contributors

# Enhancement of Plasma Burn-through Simulation and Validation in JET

# Enhancement of Plasma Burn-through Simulation and Validation in JET

Hyun-Tae Kim[1,2], W. Fundamenski[1,2], A.C.C. Sips[1,3]
and JET EFDA contributors*

***JET-EFDA, Culham Science Centre, OX14 3DB, Abingdon, UK***

*[1]Department of Physics, Imperial College London, Prince Consort Road, London, SW7 2AZ, UK*
*[2]EURATOM-CCFE Fusion Association, Culham Science Centre, OX14 3DB, Abingdon, OXON, UK*
*[3]JET-EFDA, Culham Science Centre, OX14 3DB, Abingdon, OXON, UK*
** See annex of F. Romanelli et al, "Overview of JET Results",*
*(23rd IAEA Fusion Energy Conference, Daejon, Republic of Korea (2010)).*

Preprint of Paper to be submitted for publication in
Nuclear Fusion

# Enhancement of Plasma Burn-through Simulation and Validation in JET

**Hyun-Tae Kim[1,2], W. Fundamenski[1,2], A.C.C. Sips[1,3] and EFDA-JET contributors***

JET-EFDA Culham Science Centre, Abingdon, OX14 3DB, UK.
[1]Department of Physics, Imperial College London, Prince Consort Road, London, SW7 2AZ, UK
[2]EURATOM/CCFE Fusion Association, Abingdon, OX14 3DB, UK
[3]JET-EFDA, Culham Science Centre, Abingdon, OX14 3DB, UK
*See annex to F. Romanelli et al, Fusion Energy 2010 (Proc. 23rd IAEA Conf., Deajeon, 2010) IAEA Vienna.

E-mail: hyun.kim09@imperial.ac.uk

**Abstract.**

In this paper, a new burn-through model is introduced in detail, and the quantative validation of the simulation results against JET data is presented for the first time. In order to calculate the particle confinement time, a dynamic effective connection length model including an eddy current effect is used assuming ambipolar transonic transport and Bohm diffusion model for parallel and perpendicular particle losses, respectively. Plasma-Surface Interaction (PSI) effect is treated with an impurity sputtering yield and an exponential decay model of the deuterium recycling coefficient. The rate and power coefficients in the Atomic Data and Analysis Structure (ADAS) package are adopted to solve energy and particle balance. The neutral screening effects are taken into account according to particle species, and the sophisticated energy and particle balances are presented. The new burn-through simulation shows good agreement against carbon wall JET data. This indicates that the burn-through simulation can be applied to investigate the key aspect of physics in plasma burn-through and to perform a predictive simulation for ITER start-up.

## 1. Introduction

### *1.1. Motivation*

Tokamak start-up consists of the plasma break-down phase, the plasma burn-through phase, and the subsequent ramp-up process of plasma current $I_p$ until it arrives at flat-top state[1].

Plasma break-down can be explained by the Townsend avalanche theory[2]. The required electric field $E[Vm^{-1}]$ for plasma break-down at a given prefill gas pressure $p$ and effective connection length $L_f$ is calculated with the Townsend criterion,

$$E[Vm^{-1}] \geq \frac{1.25 \times 10^4 p[Torr]}{\ln(510 p[Torr] L_f[m])}. \tag{1.1}$$

ITER plasma break-down has also been evaluated using the Townsend criterion in the ITER physics basis in 1999[1].

However, the Townsend criterion suggests the condition for the initiation of electron avalanche. It is not sufficient to explain all non-sustained break-down shots where $I_p$ does not increase. In order for $I_p$ to increase, deuterium and impurities must be sufficiently ionized in the burn-through phase so that the ohmic heating power exceeds the total electron power losses resulting mainly from collisional radiation and ionization.

In present tokamaks, the required loop voltage in the burn-through phase, *the burn-through criterion*, is usually higher than that for plasma break-down[1]. Therefore, when designing a new device or determining operation parameters, the burn-through criterion must be evaluated as well as the Townsend criterion. There were over 100 non-sustained break-down shots in JET experiments in 2009. By understanding the key physics aspects in the burn-through phase, these start-up failures can be reduced.

Furthermore, in ITER, the allowable toroidal electric field for start-up is limited up to $0.3[V/m]$ due to the engineering issues resulting from the use of superconducting poloidal coils and a continuous vacuum vessel[3]. Since tokamak start-up using such a low $E$ field requires a narrow range of prefill gas pressure, low magnetic error fields, and low impurity content, ECH-assisted start-up has been proposed for reliable start-up in ITER[3]. In order to estimate the required ECH power, a complete understanding of plasma burn-through is necessary.

### *1.2. Background*

The zero dimensional energy and particle balance model for a burn-through simulation, 0D code, has been presented by B. Lloyd[4]. In the 0D code, the energy confinement time $\tau_E$ was calculated with INTOR scaling law, in which $\tau_E$ was simply proportional to electron density $n_e$, i.e. $\tau_E[s] \equiv 5 \times 10^{-21} \tau_0 n_e[m^{-3}]$ where $\tau_0$ is a multiplier($\tau_0 \approx 0.2 \sim 2$). In addition, the particle confinement time $\tau_p$ was treated as a constant parameter($\tau_p \approx 5 \sim 50[ms]$).

The impurity content, which is one of the important parameters determining the burn-through criterion, was assumed to be constant in the 0D code. The evolution of an

impurity content in a plasma was treated in the SCENPLINT code with an exponentially growing function, i.e. $n_c/n_e \equiv 0.013 + 0.03((1 - exp(-t[s]/0.25)))$ [5],[6],[3].

### *1.3. Brief explanation of the new models*

One of the crucial features in the burn-through phase is the transition of magnetic field configuration, i.e. the change from the open field line configuration to the closed flux surfaces (CFS). This transition results in the change of dominant particle loss mechanism, i.e. the change of dominant particle loss to perpendicular transport from parallel transport, hence, the dynamics of effective connection length must be modelled as well. In addition, the previous treatments of impurities were overly simplified. The increasing impurity content in the plasma is significantly affected by the wall material and ion transport. Therefore, *Plasma-Surface Interaction (PSI)* must be included with more sophisticated models. In order to model the impurity evolution in the burn-through phase, new models of particle transport and plasma-surface interaction(PSI) have been added to B. Lloyd's model.

In the new burn-through simulation, it is assumed that a parallel particle loss in the burn-through phase is dominated by a convective transonic ambipolar flow along a magnetic field line to the vessel wall as used in divertor-SOL plasma simulations[7]. Accordingly, parallel transport losses are calculated with a finite effective connection length $L_f$ and an ion sound speed $C_s$. Regarding the perpendicular particle loss, the Bohm diffusion model is adopted. The particle confinement time is calculated by combining these transport mechanisms. The details of the calculation will be presented in section 2.4.4.

In the burn-through phase where magnetic field configuration is in transition, the evolution of an effective connection length is important for parallel particle transport. In the case of JET, it is generally observed that magnetic configuration forms closed magnetic surfaces at around 100 $[kA]$ plasma current. According to this, the evolution of an effective connection length is modelled with an exponential term approaching an infinite value from 100 $[kA]$ of plasma current. In addition, once a toroidal electric field is induced for plasma break-down, there can be significant eddy currents, thereby decreasing the effective connection length. In JET, most eddy currents in this phase flow through the support ring of the divertor tiles (MK2) due to its relatively low electric resistance. This effect is considered with a two ring model, i.e. plasma current ring and MK2 current ring.

Plasma-Surface Interaction is modelled with a wall-sputtering yield according to the kind of incident ions. In the carbon-wall JET where chemical sputtering was dominant, a carbon sputtering yield due to a deuterium ion or an oxygen ion can be assumed to be constant based on experimental data[8]. The recycling coefficient of incident deuterium ions is modelled with an exponential decay function since the total amount of deuterium atoms attached on the wall will be decreasing as a wall-sputtering process proceeds. Recycling coefficients of impurities, i.e. carbon and oxygen, are assumed to

be 0 and 1, respectively, according to their volatility.

Another important feature in the burn-through phase is a low electron temperature, less than 100$[eV]$. This requires sophisticated calculations of atomic reactions in each ionic charge state of a deuterium and impurities. By using the *Atomic Data and Analysis Structure (ADAS)* rate and power coefficients[9], energy and particle balance equations in each ionic charge state of a deuterium and impurities are solved in matrix form. As electron temperature increases in the burn-through phase, the mean free path for neutral ionization decreases, thereby reducing the neutral volume within a plasma. This neutral screening effect is taken into account according to particle species. These more sophisticated energy and particle balances will be presented in section 2.

Even though the plasma burn-through has been simulated previously[4][5][10], quantative validation of the models against experimental data has not been published extensively. One of the main limitations are the available tokamak diagonostic data, together with an adaquate model to provide the simulations. In order to test whether the model incorporates the key aspects of plasma burn-through physics, its validation process is necessary. This is also important for further applications such as ECH heating power modulation for ECH-assisted start-up[11] and ferromagnetic effects in superconducting tokamak start-up[12], all of which are based on the burn-through simulation. Validation of the new burn-through model against JET experimental data will be presented in section 3.

### *1.4. Structure of the article*

The scope of this paper is to present the new model and give a quantative validation against experimental data. In section 2, the theoretical models for the new burn-through simulation are given in detail. In section 3, quantative validation of the new burn-through simulation against JET experimental data is introduced. In section 4, the potential applications and the limitations of the model are discussed. In section 5, conclusions are presented.

## 2. Theoretical model for burn-through simulation

In this article, all physical quantities are expressed in SI units except for the plasma temperature and the prefill gas pressure. A plasma temperature and a prefill gas pressure are indicated in $[eV]$ and $[Torr]$, respectively. In exceptional cases, an additional explanation is attached.

### *2.1. Circuit Equation for plasma current*

When a loop voltage is applied by a transformer action in Tokamaks, an eddy current is induced in the vessel since the electric resistance of the vessel is comparable with that of plasma column. Until the plasma resistance becomes much smaller than the vessel's electric resistance, the amount of eddy current can be significant. In the case of JET,

the MK2 ring, which is a divertor mechanical support structure, has the lowest electric resistance. The MK2 current $I_{MK2}$ and plasma current $I_p$ can be modelled with a two ring model,

$$V_l = I_p R_p + L_p \frac{dI_p}{dt} + M \frac{dI_{MK2}}{dt} \tag{2.1}$$

$$V_l = I_{MK2} R_{MK2} + L_{MK2} \frac{dI_{MK2}}{dt} + M \frac{dI_p}{dt} \tag{2.2}$$

where $V_l$ is an applied loop voltage. $L_p$ and $L_{MK2}$ are self-inductances of a plasma current ring and the MK2 current ring. Similarly, $R_p$ and $R_{MK2}$ indicate their resistances, respectively. $M$ represents a mutual inductance between the two current rings.

The plasma inductance $L_p$ is a function of plasma major radius $R$, minor radius $a$, and internal inductance $l_i$[4],

$$L = \mu_0 R(\ln \frac{8R}{a} + \frac{l_i}{2} - 2). \tag{2.3}$$

In Equation (2.3), internal inductance $l_i$ can be calculated using [13]

$$l_i = \frac{2\int_0^a B_\theta^2 r dr}{a^2 B_{\theta a}^2}. \tag{2.4}$$

In the case of a flat $I_p$ profile which is assumed in the model, $l_i$ is equal to 0.5. In Equation (2.1), $R_p$ indicates plasma resistance which can be calculated with Spitzer resistivity[13],

$$R_p = 5 \times 10^{-5} \times \ln\Lambda \times Z_f \times \frac{2R}{a^2} \times T_e^{-\frac{3}{2}} \tag{2.5}$$

where $\ln\Lambda$ is Coulomb logarithm and $Z_f$ represents an effective charge. $Z_f$ is defined as [13]

$$Z_f = \frac{\sum_A \sum_z n_A^{z+} z^2}{\sum_A \sum_{z\geq 1} n_A^{z+} z}, \tag{2.6}$$

where subscript $A$ represents a deuterium or an impurity. $z$ means an ionic charge state. Accordingly, $n_A^{z+}$ indicates deuterium ion density $n_D^{1+}$ or impurity ion densities $n_I^{z+}$ of which the charge state is z.

The value of the inductances and the resistances for JET are summarized in Table 1. It should be noted that plasma resistance $R_p$ is a function of electron temperature $T_e$ and effective charge $Z_f$. In order to calculate $I_p$ with Equation (2.1) and (2.2), $T_e$ and $Z_f$ should be obtained by solving the energy and particle balance equations.

### *2.2. Electron Energy Balance*

The electron energy balance equation is

$$\frac{3}{2}\frac{d(n_e e T_e)}{dt} = P_{oh} + P_{aux} - (P_{iz} + P_{rad}) - P_{equi} - P_{conv}^e. \tag{2.7}$$

In this model, it is assumed that there is no auxiliary heating source, i.e. $P_{aux} = 0$ . $P_{oh}$ is the only electron heating source, and all ohmic heating power is assumed to be

absorbed by electrons without ion heating. Ohmic heating power per unit volume is

$$P_{oh} = \frac{I_p^2 R_p}{V_p}, \tag{2.8}$$

where $V_p$ is the plasma volume[4]. Electron power losses in Equation (2.7) consist of collisional ionization power loss $P_{iz}$, radiation power loss $P_{rad}$, equilibration power loss $P_{equi}$, and convective transport power loss $P^e_{conv}$.

Collisional ionization process is a power loss mechanism from an electron point of view since a free electron loses their kinetic energy as much as the binding energy of an electron in an atom[4]. Therefore, collisional ionization power loss $P_{iz}$ is

$$P_{iz} = \frac{V_n^A}{V_p} \sum_A \mathcal{R}^{0\to 1+}_{A,iz} W_A^{0\to 1+} n_e n_A^0 + \sum_A \sum_{z\geq 1} \mathcal{R}^{z+\to(z+1)+}_{A,iz} W_A^{z+\to(z+1)+} n_e n_A^{z+}, \tag{2.9}$$

where $W_A^{z+\to(z+1)+}$ is its ionization energy required to ionize an atom or a non-fully ionized ion from $z+$ to an $(z+1)+$. Here $V_n^A$ represents a neutral volume of species $A$ within a plasma volume. The details of the neutral screening effect will be discussed in section 2.4.2.

The reaction rate coefficients and power coefficients are expressed as $\mathcal{R}$ and $\mathcal{P}$. Their superscript indicates the change of the ion charge in the atomic reaction, the subscripts represent the species of the reaction particle and the kind of the reaction. For example, $\mathcal{R}^{z+\to(z-1)+}_{A,rec}$ indicates a recombination rate coefficient of species $A$ of which the ionic charge transits to $(z-1)+$ from $z+$ through a recombination reaction. In the case of ionization and charge exchange, the subscripts are $iz$ and $rec$, respectively. $\mathcal{P}^{z+}_{A,line}$ is a power coefficient of line radiation and $\mathcal{P}^{z+\to(z-1)+}_{A,RB}$ is a power coefficient of Recombinations and Bremsstrahlung radiation. The rate coefficients and power coefficients used in the burn-through simulation are obtained from ADAS. Further information about this is available in H. P. Summers's paper published in 2006[9].

If there is a collisional excitation of an atom or an ion, a free electron also loses its kinetic energy. In the case of optically thin plasma, which is assumed in this article, the amount of the electron power loss for collisional excitations is equal to the subsequent line radiation power[4]. The electron power loss resulting from the electron deceleration due to the background ions is also equal to the bremsstrahlung radiation power loss [4]. However, in the case of recombinations, the radiation power loss is greater than the electron power loss for recombination reactions since the potential energy in an atom or an ion is included in the total recombination radiation power[4]. Therefore, this amount must be extracted from the total recombination radiation power in order to calculate the electron power loss. The total electron power loss through radiation is

$$\begin{aligned} P_{rad} = &\sum_A \frac{V_n^A}{V_p} \mathcal{P}^0_{A,line} n_e n_A^0 \\ &+ \sum_A \sum_{z\geq 1} (\mathcal{P}^{z+}_{A,line} + \mathcal{P}^{z+\to(z-1)+}_{A,RB} - \mathcal{R}^{z+\to(z-1)+}_{A,rec} W_A^{(z-1)+\to z+}) n_e n_A^{z+}. \end{aligned} \tag{2.10}$$

Electrons also lose energy through elastic coulomb collisions with ions, equilibration.

The equilibration power loss $P_{equi}$ is well known as

$$P_{equi} = 7.75 \times 10^{-34}(T_e - T_i)\frac{n_e \ln \Lambda}{T_e^{3/2}}(\sum_A \sum_{z\geq 1} \frac{n_A^{z+} z^2}{M_A}), \tag{2.11}$$

where $M_A$ is ion mass of each species in $amu$[4].

Electron convective transport power loss $P_{conv}^e$ is

$$P_{conv}^e = \frac{3}{2}\frac{n_e e T_e}{\tau_e}, \tag{2.12}$$

where electron confinement time $\tau_e$ is assumed to be equal to deuterium confinement time $\tau_D$ in this model. The details of particle confinement time will be discussed in section 2.4.4.

### *2.3. Ion Energy Balance*

The ion energy balance equation is[4]

$$\frac{3}{2}(n_i e T_i) = P_{equi} - P_{CX} - P_{conv}^i. \tag{2.13}$$

where ion density $n_i$ and temperature $T_i$ are defined to be

$$\begin{aligned} n_i &= n_D^{1+} + \sum_I \sum_{z\geq 1} n_I^{z+} \\ T_i &= T_D^{1+} = T_I^{z+}. \end{aligned} \tag{2.14}$$

Ions are assumed to be heated only by equilibration with electrons and lose energy through charge exchange reactions and ion convective transport[4]. The ion energy loss in a charge exchange reaction is equal to the energy difference between the energetic ion (a deuterium ion or an impurity ion) and the lower-energy deuterium atom[4], which is assumed to be at room temperature, i.e. $T_0 = 0.026[eV]$. In this model, deuterium is assumed to be the only electron donor for charge exchange reactions. Therefore, charge exchange reaction occurs only in a deuterium neutral volume within a plasma volume, $V_n^D$. Accordingly, the ion power loss due to a charge exchange reaction is

$$P_{cx} = \frac{V_n^D}{V_p}(\frac{3}{2} n_D^0 e(T_i - T_0) \sum_A \mathcal{R}_{A,cx}^{1+\rightarrow 0} n_A^{1+}). \tag{2.15}$$

Ion convective transport power loss $P_{conv}^i$ can be calculated as

$$P_{conv}^i = \sum_A \sum_{z\geq 1} \frac{3}{2}\frac{n_A^{z+} e T_i}{\tau_D}. \tag{2.16}$$

### *2.4. Deuterium Particle Balance*

*2.4.1. Deuterium recycling coefficient model* Once deuterium ions arrive at the vessel wall, they are recycled according to the recycling coefficient $Y_D^D$. In the burn-through phase, this deuterium recycling coefficient can be higher than 1 since deuterium atoms

attached on the wall are sputtered. As deuterium sputtering process proceeds, the recycling coefficient approaches 1. In order to take this change of deuterium recycling coefficient into account, an exponential decay function of deuterium recycling coefficient is used as shown below.

$$Y_D^D = c_1 - c_2(1 - exp(-\frac{t}{c_3})) \tag{2.17}$$

According to Equation (2.17), the deuterium recycling coefficient changes to $c_1 - c_2$ from $c_1$ with time $t$, and the rate of the change is determined by $c_3$.

*2.4.2. Neutral screening effect* As electron temperature increases, the ionization mean-free-path of neutrals, $\lambda_{A,iz}$, is reduced, thereby preventing neutrals from penetrating into a plasma column, i.e. decrease in the neutral volume within a plasma column, $V_n^A$. This neutral screening effect requires sophisticated particle balance equations. For example, a charge exchange reaction is only available in a deuterium neutral volume within a plasma volume, $V_n^D$, since a deuterium atom is assumed to be the only electron donor in this article. In addition, ionization and excitation of neutral $A$ are limited to $V_n^A$ which contains neutral $A$.

The neutral screening effect has been modelled in B. Lloyd's model[4]. However, the different neutral volume between impurities was not taken into account in the model. In addition, $V_n^A$ is likely to be a function of the cross-section of a neutral volume as shown in Figure 1 rather than a simple proportional function of $\lambda_{A,iz}$, assumed in [4]. We define the neutral volume within a plasma volume as

$$V_n^A = \begin{cases} 2\pi R(\pi\kappa a^2 - \pi\kappa(a - \lambda_{A,iz})^2) & \text{if } \lambda_{A,iz} \leq a \\ V_p & \text{if } \lambda_{A,iz} > a \end{cases}$$

where $\kappa$ is the elongation of plasma cross-section.

For the sake of a compact expression, the neutral volume coefficient is defined as $\gamma_n^A$,

$$\gamma_n^A = 1 - \frac{V_p - V_n^A}{V_V}, \tag{2.18}$$

i.e. the total neutral volume including the volume within a plasma is $\gamma_n^A V_V$.

*2.4.3. Dynamic effective connection length model* Effective connection length without a plasma current is calculated with [14]

$$L_f = 0.25 \times a\frac{B_\phi}{B_z}.$$

However, this should be modified as a function of plasma current to simulate the burn-through phase as one of the important features in this phase is the formation of CFS i.e. a significant change of the effective connection length $L_f$. Since the mechanism of

the dominant particle loss, i.e. a parallel or perpendicular transport, is subject to $L_f$, the dynamic model of $L_f$ is of crucial importance.

It is generally accepted that a magnetic field configuration becomes closed with increasing plasma current. In the case of JET, the plasma current from which the field transition occurs is around 100 [kA]. Based on this, the $L_f$ is modelled as a function of plasma current with $I_{ref} = 100[kA]$,

$$L_f = 0.25 \times a(t)\frac{B_\phi}{B_z(t)}exp(\frac{I_p(t)}{I_{ref}}) \tag{2.19}$$

where $B_\phi$ and $B_z(t)$ are a toroidal field and a stray field, respectively. $B_z(t)$ is composed of vertical field $B_v$ and error field $B_{eddy}$, due to the eddy current in a vacuum vessel in JET. The total stray field $B_v$ at JET is approximately $10^{-3}[T]$ at $t = 0[s]$. The contribution of $B_{eddy}(t)$ near the middle point between the centre of a plasma column and the position of the MK2 structure can be approximately calculated as,

$$B_{eddy}(t) = \frac{\mu_0}{2\pi}I_{MK2}(t).$$

*2.4.4. Particle confinement time* For an open field configuration, the parallel transport loss can be assumed as a transonic ambipolar flow along a magnetic field line toward the vessel wall. Analogous to the plasma in the *Scrape-Off-Layer (SOL)*, deuterium confinement time due to the parallel particle loss $\tau_{D,\parallel}$ is calculated by dividing effective connection length $L_f$ by the deuterium ion sound speed $C_s$,

$$\tau_{D,\parallel} = \frac{L_f}{C_s}, \tag{2.20}$$

where

$$C_s = \sqrt{\frac{eT_e + eT_i}{m_D}}, \tag{2.21}$$

where $m_D$ is deuterium ion mass, $2 \times 1.66 \times 10^{-27}$ in $[kg]$.

While perpendicular particle loss is small enough to be ignored when $L_f$ is sufficiently short, the perpendicular particle transport becomes dominant as field lines are closed. In this model, Bohm diffusion is adopted to calculate the perpendicular particle transport[15]. The Bohm diffusion velocity is presented in [16],

$$v_{Bohm}(t) = \frac{2D_{Bohm}(t)}{a(t)} \tag{2.22}$$

where

$$D_{Bohm}(t) = \frac{1}{16}\frac{T_e}{B_\phi}. \tag{2.23}$$

Accordingly, the particle confinement time due to the perpendicular transport is

$$\tau_{D,\perp} = \frac{a(t)}{v_{Bohm}(t)}exp(\frac{a(t)}{\lambda_{ii}(t)}) \tag{2.24}$$

In Equation (2.24), exponential term is attached to include the ion-ion collision effect[15] where a mean free path for ion-ion collision is given by[7]

$$\lambda_{ii}(t) = \frac{10^{16} T_i(t)^2}{n_i(t)}. \tag{2.25}$$

The confinement time of a deuterium ion $\tau_D$ is then obtained with Equation (2.20) and (2.24) as

$$\frac{1}{\tau_D} = \frac{1}{\tau_{D,\parallel}} + \frac{1}{\tau_{D,\perp}}. \tag{2.26}$$

*2.4.5. Modified deuterium balance* The above modifications are summarized in the following particle balance equation of a deuterium atom and ion.

Particle balance equation of deuterium atom:

$$\begin{aligned}\frac{dn_D^0}{dt} = \frac{1}{\gamma_n^D V_V}(&V_p \mathcal{R}_{D,rec}^{1+\to 0} n_e n_D^{1+} \\ &- V_n^D \mathcal{R}_{D,iz}^{0\to 1+} n_e n_D^0 - V_n^D \sum_I \sum_{z\geq 1} \mathcal{R}_{I,cx}^{z+\to(z-1)+} n_D^0 n_I^{z+}) + \frac{\Gamma_{D,in}^{total}}{\gamma_n^D V_V},\end{aligned} \tag{2.27}$$

where the total influx of deuterium atoms $\Gamma_{D,in}^{total}$ is

$$\Gamma_{D,in}^{total} = V_p \frac{Y_D^D n_D^{1+}}{\tau_D}. \tag{2.28}$$

Particle balance equation of deuterium ions:

$$\frac{dn_D^{1+}}{dt} = \frac{V_n^D}{V_p} \mathcal{R}_{D,iz}^{0\to 1+} n_e n_D^0 - \mathcal{R}_{D,rec}^{1+\to 0} n_e n_D^{1+} + \frac{V_n^D}{V_p} \sum_I \sum_{z\geq 1} \mathcal{R}_{I,cx}^{z+\to(z-1)+} n_D^0 n_I^{z+} - \frac{n_D^{1+}}{\tau_D}. \tag{2.29}$$

*2.5. Impurity Particle Balance*

It is generally accepted that the electron power losses for radiations and ionizations, i.e. $P_{rad} + P_{iz}$, are dominant in the total electron power loss during the burn-through phase. Since $P_{rad} + P_{iz}$ are significantly affected by impurity content[3], a treatment for impurity evolution is of crucial importance.

In the burn-through phase, there is considerable impurity sputtering and recycling[1], that affect impurity evolution in the plasma. In order to take them into account, impurity transport and PSI effects are included in the model.

In this article, $Y_A^I$ represents an impurity sputtering yield(or a recycling coefficient) due to a deuterium or impurity ion bombardment. Here, superscript $I$ indicates sputtered (or recycled) impurity, i.e. carbon or oxygen, and subscript $A$ represents an incident ion.

*2.5.1. Plasma Surface Interaction model* If a deuterium or an impurity ion strike a vessel wall, impurity atoms are ejected from the wall through sputtering or recycling[7]. The species of a dominant impurity is subject to the wall material. In the Carbon-wall JET experiments, hydrocarbon such as $CD_4$ is a major impurity[7].

While a physical sputtering yield is a function of incident ion energy[7], a chemical sputtering yield is weakly dependent on incident ion energy. In the carbon wall, chemical sputtering dominates physical sputtering when incident deuterium ion energy is lower than $100[eV]$[8] which is a typical ion temperature in the burn-through phase. In addition, in laboratory plasma experiments, the carbon sputtering yield due to the low-energy deuterium ion bombardment, $Y_D^C$, has been measured to be less than 0.03[8] when a substrate temperature is around $500[K]$[8], which is similar to the wall temperature in JET. Based on this, $Y_D^C$ in the burn-through simulation of the Carbon-wall JET is assumed to be a constant parameter of 0.03.

Oxygen is another primary intrinsic impurity in tokamaks. Oxygen is not only a strong radiator in a plasma, but also it can lead to a high level of carbon content[7]. When there is an oxygen bombardment on carbon wall with an energy of a several tens of $eV$, carbon monoxide $CO$ is emitted dominantly with about 1.0 sputtering yield [17]. Therefore, it is assumed that an oxygen atom and a carbon atom are ejected from the wall by oxygen ion bombardment, i.e. $Y_O^O \equiv 1.0$ and $Y_O^C \equiv 1.0$.

Once impurity ions arrive at the vessel wall, they are assumed to be recycled to a neutral impurity according to their recycling coefficient $Y_I^I$ which is the same for all ionic charge states. The oxygen recycling coefficient, $Y_O^O$, and the carbon recycling coefficient, $Y_C^C$, are assumed to be 1 and 0, respectively, according to their volatility. The sputtering yields and recycling coefficients used in the model are summarized in Table 2.

*2.5.2. Impurity Transport model* The parallel flow velocity of impurities at sheath entrance $v_z$ during the burn-through phase is assumed to be the deuterium ion sound speed $C_s$. Justification of this assumption is given in the Appendix. According to the assumption, impurity confinement time due to parallel transport $\tau_{I,\parallel}$ is also equal to $\tau_{D,\parallel}$ in the model, i.e. $\tau_{I,\parallel} = \tau_{D,\parallel}$.

Since Bohm diffusion coefficient $D_{Bohm}$ is only dependent on an electron temperature, it is valid for impurities as well. Accordingly, this results in the same diffusion particle loss of impurities with deuterium ion's, i.e. $\tau_{I,\perp} = \tau_{D,\perp}$. Therefore, the resulting impurity confinement time is equal to the deuterium confinement time in the model, i.e.

$$\tau_I = \tau_D. \tag{2.30}$$

In the model, all influx of impurity atom results from wall sputtering or recycling due to the outflux of deuterium and impurity ions toward the wall, i.e. no gas pumping

and puffing. The total impurity influx and outflux (atoms per second) are defined to be

$$\Gamma^0_{I,in} = V_p \sum_A \sum_{z\geq 1} \frac{Y^A_I n^{z+}_A}{\tau_I}, \tag{2.31}$$

$$\Gamma^{z+}_{I,out} = V_p(\frac{n^{z+}_I}{\tau_I}). \tag{2.32}$$

*2.5.3. Impurity particle balance* The general form of modified impurity particle balance equations including the neutral screening effect and PSI effects is shown below.

$$\frac{dn^0_I}{dt} = -\frac{V^I_n}{\gamma^I_n V_V}\mathcal{R}^{0\to 1+}_{I,iz} n_e n^0_I + \frac{V_p}{\gamma^I_n V_V}\mathcal{R}^{1+\to 0}_{I,rec} n_e n^{1+}_I + \frac{V^D_n}{\gamma^I_n V_V}\mathcal{R}^{1+\to 0}_{I,cx} n^0_D n^{1+}_I + \frac{\Gamma^0_{I,in}}{\gamma^I_n V_V} \tag{2.33}$$

$$\begin{aligned}\frac{dn^{1+}_I}{dt} = {} & \frac{V^I_n}{V_p}\mathcal{R}^{0\to 1+}_{I,iz} n_e n^0_I - \mathcal{R}^{1\to 2+}_{I,iz} n_e n^{1+}_I + \mathcal{R}^{2+\to 1+}_{I,rec} n_e n^{2+}_I - \mathcal{R}^{1+\to 0}_{I,rec} n_e n^{1+}_I + \frac{V^D_n}{V_p}\mathcal{R}^{2+\to 1+}_{I,cx} n^0_D n^{2+}_I \\ & - \frac{V^D_n}{V_p}\mathcal{R}^{1+\to 0}_{I,cx} n^0_D n^{1+}_I - \frac{n^{1+}_I}{\tau_I}\end{aligned} \tag{2.34}$$

$$\begin{aligned}\frac{dn^{z+}_I}{dt} = {} & \mathcal{R}^{(z-1)+\to z+}_{I,iz} n_e n^{(z-1)+}_I - \mathcal{R}^{z+\to(z+1)+}_{I,iz} n_e n^{z+}_I + \mathcal{R}^{(z+1)+\to z+}_{I,rec} n_e n^{(z+1)+}_I - \mathcal{R}^{z+\to(z-1)+}_{I,rec} n_e n^{z+}_I \\ & + \frac{V^D_n}{V_p}\mathcal{R}^{(z+1)+\to z+}_{I,cx} n^0_D n^{(z+1)+}_I - \frac{V^D_n}{V_p}\mathcal{R}^{z+\to(z-1)+}_{I,cx} n^0_D n^{z+}_I - \frac{n^{z+}_I}{\tau_I}\end{aligned} \tag{2.35}$$

The corresponding matrix for impurity particle balance is shown below.

$$\frac{d}{dt}\begin{pmatrix} n^0_I \\ n^{1+}_I \\ n^{2+}_I \\ \vdots \end{pmatrix} = \begin{pmatrix} \mathbb{A} & \mathbb{B} & 0 & 0 & \dots \\ \mathbb{C} & \mathbb{D} & \mathbb{E} & 0 & \dots \\ 0 & \mathbb{F} & \mathbb{G} & \mathbb{H} & \dots \\ \vdots & \vdots & \vdots & \ddots & \end{pmatrix}\begin{pmatrix} n^0_I \\ n^{1+}_I \\ n^{2+}_I \\ \vdots \end{pmatrix} + \begin{pmatrix} \frac{\Gamma^0_{I,in}}{V_V} \\ 0 \\ 0 \\ \vdots \end{pmatrix}$$

where

$$\mathbb{A} = -\frac{V_p}{\gamma^I_n V_V}\mathcal{R}^{0\to 1+}_{I,iz} n_e$$

$$\mathbb{B} = \frac{V_p}{\gamma^I_n V_V}\mathcal{R}^{1+\to 0}_{I,rec} n_e + \frac{V^D_n}{\gamma^I_n V_V}\mathcal{R}^{1+\to 0}_{I,cx} n^0_D$$

$$\mathbb{C} = \frac{\gamma^I_n V_V}{V_p}\mathcal{R}^{0\to 1+}_{I,iz} n_e$$

$$\mathbb{D} = -\mathcal{R}^{1+\to 2+}_{I,iz} n_e - \mathcal{R}^{1+\to 0}_{I,rec} n_e - \frac{V^D_n}{V_p}\mathcal{R}^{1+\to 0}_{I,cx} n^0_D - \frac{1}{\tau_I}$$

$$\mathbb{E} = \mathcal{R}^{2+\to 1+}_{I,rec} n_e + \frac{V^D_n}{V_p}\mathcal{R}^{2+\to 1+}_{I,cx} n^0_D$$

$$\mathbb{F} = \mathcal{R}^{1+\to 2+}_{I,iz} n_e$$

$$\mathbb{G} = -\mathcal{R}^{2+\to 3+}_{I,iz} n_e - \mathcal{R}^{2+\to 1+}_{I,rec} n_e - \frac{V^D_n}{V_p}\mathcal{R}^{2+\to 1+}_{I,cx} - \frac{1}{\tau_I}$$

$$\mathbb{H} = \mathcal{R}^{3+\to 2+}_{I,rec} n_e + \frac{V^D_n}{V_p} \mathcal{R}^{3+\to 2+}_{I,cx} n^0_D \tag{2.36}$$

*2.6. Electron particle Balance*

On the condition of charge neutrality, an electron density is calculated using each ion density[4],

$$n_e = \sum_A \sum_{z\geq 1} z n^{z+}_A. \tag{2.37}$$

## 3. Validation of burn-through simulation in Carbon-wall JET

*3.1. Diagnostic tools used for validation*

Figure 2 shows EFIT data for the plasma equilibrium and the lines of sight of the diagnostic tools, which are used for validation of the model in JET. The total radiation power loss is obtained with bolometry measurement. Thomson scattering data is used for the volume-averaged value of an electron temperature and density. Interferometry data is used for the volume-averaged value of an electron density. The emission rate of photons which have a specific wavelength(465[$nm$] for $C^{2+}$) are measured by photomultiplier tubes of which the lines of sight are vertical and horizontal, respectively, as shown in Figure 2. The data of $C^{2+}$ are averaged using the two measurements of the different line of sight.

*3.2. Initial conditions for burn-through simulation*

In order to perform simulations with the model, initial conditions should be given at the starting point of the burn-through phase, i.e. the end of the electron avalanche. R. Papoular has defined electron avalanche(plasma break-down) as the realization of a critical electron density $n_{ec}$, from which coulomb collisions dominate atomic and molecular collisions[18]. Based on this, the initial values required for the burn-through simulation in JET are given for the plasma parameters at the transition of the dominant collisions.

According to the definition of the electron avalanche, the degree of ionization at the transition can be calculated:

$$n_{ec}\sigma_{e-i} = (n_a - n_{ec})\sigma_{e-a} \tag{3.1}$$

where $n_a$ is the neutral density. The cross-section for electron-ion collision $\sigma_{e-i}$ and electron-atom collision $\sigma_{e-a}$ are[18]

$$\sigma_{e-i} \approx 1.5 \times 10^{-16} T_e^{-2} \tag{3.2}$$

$$\sigma_{e-a} \approx 3 \times 10^{-19} T_e^{-0.5}. \tag{3.3}$$

The degree of ionization where the electron density is $n_{ec}$ is

$$\frac{n_{ec}}{n_a - n_{ec}} = \frac{\sigma^{cr}_{e-a}}{\sigma^{cr}_{e-i}} \approx \frac{3 \times 10^{-19} T^{-0.5}_{ec}}{1.5 \times 10^{-16} T^{-2}_{ec}} = 2 \times 10^{-3} T^{\frac{3}{2}}_{ec} \tag{3.4}$$

where the $T_{ec}$ is the electron temperature at which the critical electron density $n_{ec}$ is achieved. If we assume $T_{ec}$ is approximately $1[eV]$, then the consistent degree of ionization is

$$\frac{\gamma_c}{1-\gamma_c} \approx \gamma_c \approx 0.002 \tag{3.5}$$

where $\gamma_c = n_{ec}/n_a$. Since the neutrals can be assumed to have a room temperature($\approx 0.03[eV]$), $n_{ec}$ is calculated with the initial prefill gas pressure $p$,

$$n_{ec} = 0.002 n_a \approx 0.002 \times 2.78 \times 10^{22} p[Torr] \tag{3.6}$$

where $n_a \approx 2.78 \times 10^{22} p[Torr]$. $n_{ec}$ enables us to calculate the plasma current density at the transition point with the electron drift speed $v_{De}(\approx 43E/p)$ [2],

$$J_c = e n_{ec} \times (43\frac{E}{p}) \approx 382.5 \times E[V/m]. \tag{3.7}$$

Table 3 summarizes the initial conditions for the burn-through simulation.

In order to compare the simulational result against discharge 77210, which is one of the typical burn-through shots in JET, measured loop voltage $V_{loop}(t)$(about $26[V]$ of the peak) and EFIT data such as major radius $R(t)$, minor radius $a(t)$, and plasma cross-section $A_p(t)$ of a plasma column in # 77210 shot are used as an input data in the simulation. For deuterium recycling coefficient $Y_D^D$ in Equation (2.17), $c1$, $c2$, and $c3$ are assumed to be 1.1, 0.09, and 0.1, respectively. These constants are optimized to match the simulation results with # 77210 JET data.

### *3.3. Comparison between the simulational result and JET data*

Figure 3 shows JET data and the simulational results between 0 and 0.5 second in #77210. The plasma current in the simulation and JET data start to increase with the loop voltage applied from $t = 0[s]$ onwards. Both approaches $0.8[MA]$ toward the end of the simulation at $t = 0.5[s]$ showing very good agreement.

One of the important features in the burn-through phase is the radiation peak(barrier), which results from the change of the total radiation power as shown in the bolometry data[19]. In Figure 3, the radiation barrier is reproduced in the simulation, and has a similar magnitude, about $250[kW]$, as the bolometry data. In addition, the total radiation power around the radiation barrier has a similar FWHM, and the growth rate after the radiation barrier is also similar. These imply the model reflects key aspects of physics of the radiation power during the burn-through phase.

The electron temperature and density indicated by the red solid lines in Figure 3(c)(d) are measured by Thomson scattering[20]. The simulated electron temperature and density approaches similar values with the Thomson scattering data, showing reasonable evolution. However, the simulated electron temperature and density have a discrepancy before arround 0.15 second. Probably, this is due to the the error of the EFIT data, which is used to calculate volume averaged value with the raw Thomson scattering data. There can be significant errors in the EFIT data in the early phase of

discharge such as the burn-through phase. This would result in errors in the volume-averaged values. The red dotted line in Figure 3(d) is the electron density measured by interferometry[21] in JET. Its descrepancy with the Thomson scattering data implies that there are errors in the diagnostic data.

Figure 4(a) show the number of photons emitted by $C^{2+}$. The red line is the measured values and the blue line is the synthetic data, which is calculated from the simulated plasma parameters, i.e. $n_e$, $T_e$, and $n_c^{2+}$ in Figure 4. The calculation of the synthetic data is

$$I_{C2+} = n_e n_c^{2+} \mathcal{PEC}_{C2+}(n_e, T_e)[p\ m^{-3} sec^{-1}] \tag{3.8}$$

where $\mathcal{PEC}_{C2+}(n_e, T_e)$ is a photon emissivity coefficient, which is a function of electron density and temperature. The photon emissivity coefficient for $465[nm]$ wavelength is obtained from ADAS[9].

As can be seen in Equation (3.8), since the growth and decay of $C^{2+}$ line emssion result from the change of $n_c^{2+}$, the change of photon emmision rate can give us important information about the $n_c^{2+}$ evolution. The peak value of $C^{2+}$ line emssion and its decrease after the peak point indicate that the maximum amount of $n_c^{2+}$ exist at around this time and most $C^{2+}$ are ionized to higher charge states after the peak. The synthetic photon emission rate of the $C^{2+}$ line shows a similar time scale of growth and decay with those of the measured value. It should be noted that the change of the synthetic $C^{2+}$ line emssion is available only with an adequate model for impurity evolution. The similar behaviour of the synthetic data implies the simulation can compute the evolution of $C^{2+}$ with acceptable accuracy.

In JET, observation of carbon evolution in the burn-through phase is limited to $C^{2+}$ due to the lack of diagnostic data available for this phase. The burn-through simulation can provide information of the impurities in other charge states. The simulated evolution of carbon ions is presented in Figure 4(b). As explained above, the peak of $C^{2+}$ density is coincident with that of the systnetic $C^{2+}$ line. $C^{3+}$ density increases as $C^{2+}$ density decreases, and so on. Through ionization of carbon ions, $C^{6+}$ density becomes dominant from $0.15[s]$ onwards, indicating that most carbon ions are fully ionized from from that time. Figure 4(c), enlarged from Figure 4(b), describes the process of carbon burn-through in detail.

## 4. Discussion

Model validation using the five subsequent discharges (#77211 $\sim$ 77215) has been performed. The simulations of the radiated power, electron density evolution, and $C^{2+}$ line emission show similar agreement with the measured data as shown for #77210 in Figure 3 and 4. However, the plasma current rise is slightly overestimated in the discharges. The plasma current after the burn-through phase depends on the loop voltage available. The time evolution of the loop voltage available for the plasma current build-up would require detailed information of the magnetic equilibrium. This is not

used in the model(only external measurement is used), hence the agreement with the measured plasma current rise could be improved.

In the model, a uniform plasma temperature and density are assumed(0-D). Although the simulational results show good agreement against JET data, including the effect of plasma profiles into the model would be an improvement. This would allow for quantitative investigation of power balances as both ohmic heating and power losses are functions of plasma parameters which can be different at each position. The profile effect would be also important for particle balance, due to the particle diffusions within a plasma column. Modelling of such a 1D(or 2D) effect would enable the model to describe the details of the burn-through physics as a function of the plasma radius, i.e. burn-through shell, localised heating by microwaves.

In the model, the error field are calculated only with the eddy current flowing on MK2 structure. This is a simplified model for JET. Hence, for applications to other tokamaks, a 2D(or 3D) electromagnetic code should be incorporated into the model to calculate the distributed vessel current.

It is assumed that there is no additional heating power in this article, what is the case for JET. However, various RF and NBI systems are applied in many current devices[22][23][24] during start-up, and ECH-assisted start-up has been proposed for ITER start-up[3]. In addition, non-inductive tokamak start-up, in which an additional heating power is the only heating source, is of crucial importance for a commercial fusion power plant. In order to apply the model to such issues, there is an urgent need for development of an additional heating module.

Modification of the points stated above and application to wider JET data and other tokamaks will enable the potential usage of the model to be expanded.

## 5. Conclusion

Successful plasma burn-through is necessary for tokamak start-up. If deuterium and impurities are not sufficiently ionized in the burn-through phase, it will result in a non-sustained plasma break-down. The tokamak operation parameters required for plasma burn-through are usually estimated using experimental data rather than analytical(simulational) results. In order to reduce failure shots in the current tokamaks and to attempt more reliable predictive simulation for ITER, a simulation of the plasma start-up is important.

In this article, a new burn-through model is explained in detail, and quantative validation of the model against carbon-wall JET data has been attempted for the first time. Good agreement of plasma current and the total radiation power is shown between the simulation results and JET data. Due to the errors of the measured data in the early burn-through phase, it is difficult to compare the simulated electron temperature and density. However, the simulation result and the measured densities approach the similar value with time, showing reasonable evolution. The measured photon emission rate of $C^{2+}$ are compared with the synthetic data calculated with the simulated plasma

parameters. The peak of the synthetic data is consistent with the observed peak in the measured data.

The similarity of the simulational results and JET data implies that the new burn-through model contains the essential physics in the burn-through phase. Based on this, we suggest that the model can be used to investigate the burn-through criterion in various tokamaks. In the case of beryllium wall, physical sputtering is dominant due to the low threshold energy of beryllium sputtering[7]. This will result in different plasma burn-through compared to carbon-wall tokamaks. In order for a predictive simulation of ITER start-up, modification of the PSI model for a beryllium wall is required. Validation of the modified model against ITER-Like wall JET data would enable the predictive simulation to be more reliable.

## Appendix

The parallel forces $F_z$ on an impurity for tokamak start-up can be calculated with parallel force equation. The details of the equation can be found in [7].

$$F_z = -\frac{1}{n_z}\frac{dp_z}{ds} + m_z\frac{v_D - v_z}{\tau_\parallel} + zeE + \alpha_e\frac{dT_e}{ds} + \beta_i\frac{dT_i}{ds} \tag{5.1}$$

where $v_D$ and $v_z$ are flow velocities of deuterium and impurity, respectively. Based on Spitzer's analysis on coulomb collision frequency[25], $\tau_\parallel$ is defined as a parallel collisional diffusion time,

$$\tau_\parallel \cong \frac{1.47\times 10^{13} m_z T_z (T_D/m_D)^{0.5}}{n_D z^2 \ln\Lambda}.$$

where $m_z$ is in $[amu]$ and $T$ is in $[eV]$. $\alpha_e$ and $\beta_i$ are coefficients for the electron temperature gradient force and the ion temperature gradient force, respectively[7], and they are given as a function of $z^2$[26] [27] [28],

$$\alpha_e \cong 0.71z^2$$
$$\beta_i \cong 2.6z^2.$$

In order to simplify Equation (5.1), we define some assumptions as shown below.

(i) Temperatures of electron, deuterium and impurity decrease toward the vessel wall. The values of their gradients are approximated to be

$$\frac{dT_e}{ds} \cong -\frac{T_e}{L_f}$$
$$\frac{dT_i}{ds} = \frac{dT_z}{ds} \cong -\frac{T_i}{L_f}.$$

(ii) Impurity density $n_z$ decreases toward the vessel wall and the value of the gradient are approximated to be

$$\frac{dn_z}{ds} \cong -\frac{n_z}{L_f}$$

(iii) Flow velocity of background deuterium ion is ion sound speed $C_s$

(iv) Electric field on impurity is determined by the pre-sheath potential drop.

$$E = \frac{0.7T_e}{eL_f}$$

(v) Collisionality is strong enough that the impurity inertial term can be ignored,

$$m_z \frac{dv_z}{dt} \cong 0.$$

By substituting each term in Equation (5.1) with the assumptions above, the impurity velocity $v_z$ can be derived as shown below

$$v_z = C_s + \frac{\tau_\parallel}{m_z L_f}(2T_z + 0.7zT_e - 0.71z^2T_e - 2.6z^2T_i). \tag{5.2}$$

During the burn-through phase in JET, typical plasma parameters and effective connection length $L_f$ are about

$$T_e \cong 10[eV]$$
$$T_D = T_z \cong 3[eV]$$
$$n_D \cong 10^{18}[m^{-3}]$$
$$L_f \cong 1000[m]$$
$$\ln\Lambda \cong 15.$$

With the given values, the first term, $C_s$, and the second term in Equation (5.2) are calculated to be

$$C_s \cong 25000\ [m/s]$$
$$\frac{\tau_\parallel}{m_z L_f}(2T_z + 0.7zT_e - 0.71z^2T_e - 2.6z^2T_i) \cong -5.173 + \frac{2.43}{z} + \frac{2.08}{z^2}\ [m/s]$$

As shown above, the first term, $C_s$, in Equation (5.2) dominates the second term. Therefore, for the tokamak start-up phase, impurity flow velocity $v_z$ can be assumed to be background ion's sound speed $C_s$,

$$v_z \cong C_s.$$

**Acknowledgement**

This research was funded partly by the Kwanjeong Educational Foundation and by the European Communities under the contract of Association between EURATOM and CCFE. The views and opinions expressed herein do not necessarily reflect those of the European Commission. This work was carried out within the framework of the European Fusion Development Agreement.

**REFERENCES**


[1]. Plasma Control ITER Physics Expert Group on Disruptions, MHD, Heating ITER Physics Expert Group on Energetic Particles, Current Drive, ITER Physics Expert Group on Diagnostics, and ITER Physics Basis Editors. Chapter 8: Plasma operation and control. Nuclear Fusion, **39** (12):2577, 1999.

[2]. T.S. Taylor E.A. Lazarus T.C. Luce R. Prater B. Lloyd, G.L. Jackson. Low voltage ohmic and electron cyclotron heating assisted start-up in d3d. Journal of Nuclear Fusion, **31**:2031–2053, 1991.

[3]. Y. Gribov, D. Humphreys, K. Kajiwara, E.A. Lazarus, J.B. Lister, T. Ozeki, A. Portone, M. Shimada, A.C.C. Sips, and J.C. Wesley. Chapter 8: Plasma operation and control. Nuclear Fusion, **47** (6):S385–S403, 2007.

[4]. B. Lloyd, P.G. Carolan, and C.D. Warrick. Ecrh-assisted start-up in iter. Plasma Physics and Controlled Fusion, **38** (9):1627, 1996.

[5]. V. A. Belyakov, V. I. Vasiliev, K. M. Lobanov, L. P. Makarova, and A. B. Mineev. Analysis of initial stage of plasma discharge in tokamaks: mathematical model formulation, simulation results, comparison with experiments. pages 1025–1034, 2003.

[6]. Lobanov K. M. Makarova L. P. Mineev A. B. Vasiliev V. I. Belyakov, V. A. Plasma initiation stage analysis in tokamaks with transmak code. Plasma Devices and Operations, 11:193–201, 2003.

[7]. Peter C Stangeby. The Plasma Boundary of Magnetic Fusion Devices. Institute of Physics Publishing Bristol and Philadelphia, 1999.

[8]. B.V Mech, A.A Haasz, and J.WDavis. Isotopic effects in hydrocarbon formation due to low-energy h+/d+ impact on graphite. Journal of Nuclear Materials, **255**(2-3):153–164, 1998.

[9]. H.P. Summers, W.J. Dickson, M.G. O'Mullane, N.R. Badnell, A.D. Whiteford, D.H. Brooks, J. Lang, S.D. Loch, and D.C. Griffin. Ionization state, excited populations and emission of impurities in dynamic finite density plasmas: I. the generalized collisional radiative model for light elements. Plasma Physics and Controlled Fusion, **48** (2):263, 2006.

[10]. G.G. Gladush A.D. Barkalov. Numerical simulation of the initial stage of the plasma column formation in just-t tokamak. Plasma Devices and Operations, **15**:185–192, 2007.

[11]. A. Mineev D. Morozov, A. Pshenov. Ecr heating power modulation as a means to ease the overcoming of the radiation barrier in fusion devices. Plasma Physics Reports, **36**:447–454, 2010.

[12]. Jayhyun Kim, S.W. Yoon, Y.M. Jeon, J.A. Leuer, N.W. Eidietis, D. Mueller, S. Park, Y.U. Nam, J. Chung, K.D. Lee, S.H. Hahn, Y.S. Bae, W.C. Kim, Y.K. Oh, H.L. Yang, K.R. Park, H.K. Na, and the KSTAR Team. Stable plasma start-up in the kstar device under various discharge conditions. Nuclear Fusion, **51** (8):083034, 2011.

[13]. John Wesson. Tokamaks. CLARENDON PRESS OXFORD, 2004.

[14]. J.G. Cordey J.P. Christiansen S. Ejima A. Kellman E. Lazzaro P.J. Lomas P. Morgan M.F.Nave

P. Noll A. Tanga, P.R. Thomas and F.C. Schuller. Start-up of the ohmic phase in jet. In Heinz Knoepfel, editor, Tokamak Start-up, volume 26, page 159. European Physical Society, Plenum Press, 1986.

[15]. T. Wauters, A. Lyssoivan, D. Douai, O. Marchuk, D. Wnderlich, R. Koch, G. Sergienko, G. Van Oost, and M. Van Schoor. 0d model of magnetized hydrogen-helium wall conditioning plasmas. Plasma Physics and Controlled Fusion, **53** (12):125003, 2011.

[16]. Eduardo de la Cal. Theoretical modelling of deuterium icrf wall conditioning discharges. Plasma Physics and Controlled Fusion, **48** (10):1455, 2006.

[17]. J.W. Davis and A.A. Haasz. Impurity release from low-z materials under light particle bombardment. Journal of Nuclear Materials, **241-243**:37 – 51, 1997.

[18]. R. Papoular. The genesis of toroidal discharges. Nuclear Fusion, **16**:37–45, February 1976.

[19]. A. Huber, K. McCormick, P. Andrew, P. Beaumont, S. Dalley, J. Fink, J.C. Fuchs, K. Fullard, W. Fundamenski, L.C. Ingesson, F. Mast, S. Jachmich, G.F. Matthews, Ph. Mertens, V. Philipps, R.A. Pitts, S. Sanders, and W. Zeidner. Upgraded bolometer system on jet for improved radiation measurements. Fusion Engineering and Design, **82** (5-14):1327 – 1334, 2007. ce:title Proceedings of the 24th Symposium on Fusion Technology/ce:title ce:subtitle SOFT-24/ce:subtitle.

[20]. C. Gowers M. Beurskens M. Kempenaars T. Carlstrom R. Pasqualotto, P. Nielsen and D. Johnson. High resolution thomson scattering for joint european torus (jet). Review of Scientific Instruments, **75**:3891, 2004.

[21]. L. Zabeo A. Boboc and A. Murari. Simultaneous cotton-mouton and faraday rotation angle measurements on jet. Review of Scientific Instruments, **77**:10F324, 2006.

[22]. Y.S. Bae, J.H. Jeong, S.I. Park, M. Joung, J.H. Kim, S.H. Hahn, S.W. Yoon, H.L. Yang, W.C. Kim, Y.K. Oh, A.C. England, W. Namkung, M.H. Cho, G.L. Jackson, J.S. Bak, and the KSTAR team. Ech pre-ionization and assisted startup in the fully superconducting kstar tokamak using second harmonic. Nuclear Fusion, **49** (2):022001, 2009.

[23]. J.A. Leuer, G. Cunningham, D. Mueller, N.H. Brooks, N.W. Eidietis, D.A. Humphreys, A.W. Hyatt, G.L. Jackson, J. Lohr, P.A. Politzer, R.I. Pinsker, R. Prater, P.L. Taylor, M.L. Walker, R.V. Budny, D.A. Gates, A. Nagy, S-H. Hahn, Y-K. Oh, S-W. Yoon, J.H. Yu, M. Murakami, J.M. Park, and A.C. Sontag. Solenoid-free startup experiments in diii-d. Nuclear Fusion, **51** (6):063038, 2011.

[24]. V.F. Shevchenko, M.R. O'Brien, D. Taylor, A.N. Saveliev, and MAST team. Electron bernstein wave assisted plasma current start-up in mast. Nuclear Fusion, **50**(2):022004, 2010.

[25]. Spitzer L. Physics of Fully Ionized Gases 2nd edn. New York: Wiley, 1962.

[26]. Braginskii S I. Reviews of Plasma Physics vol 1, ed M A Leontovich. New York: Consultants Bureau, 1965.

[27]. Rutherford P.H. Physics of Fluids, **17**:1782, 1974.

[28]. Chapman S. Phys. Soc., **72**:353, 1958.

| | $L[H]$ | $M[H]$ | $R[\Omega]$ |
|---|---|---|---|
| *Plasma* | $6.09 \times 10^{-6}$ | $2.49 \times 10^{-6}$ | $R_p(T_e, Z_f)$ |
| *MK2* | $9.1 \times 10^{-6}$ | $2.49 \times 10^{-6}$ | $7.5 \times 10^{-4}$ |

*Table 1: Inductances and resistances of a plasma current ring and a MK2 current ring for JET.*

| *Sputtered(recycled) atom* $\diagdown$ *incident ion* | $D^{1+}$ | $C^{z+}$ | $O^{z+}$ |
|---|---|---|---|
| $D^0$ | *Equation (2.17)* | $Y_D^C = 0$ | $Y_D^O = 0$ |
| $C^0$ | $Y_C^D = 0.03$ | $Y_C^C = 0$ | $Y_C^O = 1$ |
| $O^0$ | $Y_O^D = 0$ | $Y_O^C = 0$ | $Y_O^O = 1$ |

*Table 2: Sputtering yields and recycling coefficients.*

| *Plasma parameters* | *Initial values* |
|---|---|
| *Electron temperature* $T_e(0)$ | $1[eV]$ |
| *Ion temperature* $T_i(0)$ | $0.03[eV]$ |
| *Deuterium atom density* $n_d^0(0)$ | $2.78 \times 10^{22}\mathrm{p}[Torr]$ |
| *Electron density* $n_e(0)$ | $5.56 \times 10^{19}\mathrm{p}[Torr]$ |
| *Carbon atom density* $n_c^0(0)$ | 0 |
| *Oxygen atom density* $n_o^0(0)$ | $0.01\mathrm{n_d^0}(0)$ |
| *Plasma current density* $J_p(0)$ | $382.5 \times \mathrm{E}\,[V/m\,]$ |
| *Eddy current density* $I_{MK\ 2}(0)$ | 0 |

*Table 3: Initial conditions for the burn-through simulation in JET.*

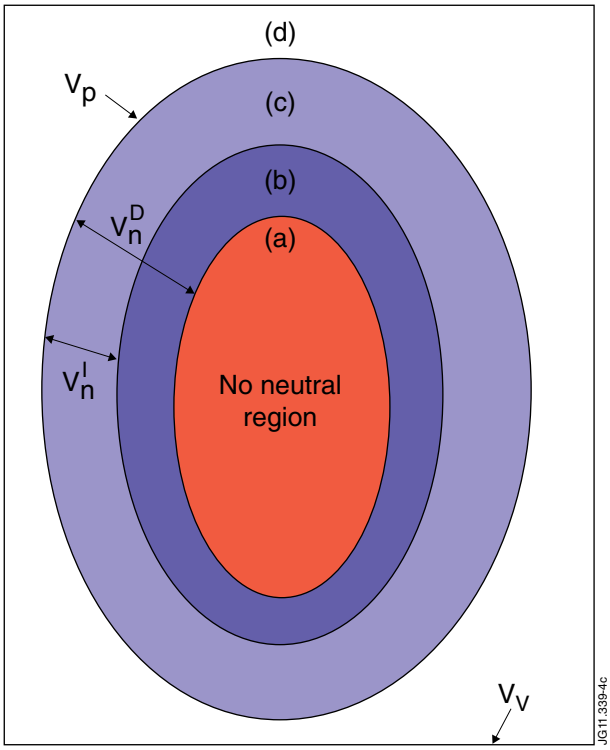


*Figure 1: The areas of blue and sky-blue indicate a neutral volume of a deuterium within a plasma volume $V_n^D$. The neutral volume of an impurity is indicated by $V_n^I$ , i.e. sky-blue region. The red region represents no neutral region into which any neutrals cannot penetrate. The sum of the two blue regions and the red area means the total plasma volume $V_p$. : (a)ions (b)ions and deuterium neutrals (c)ions and neutrals of an impurity and a deuterium (d)neutrals of impurities and a deuterium*

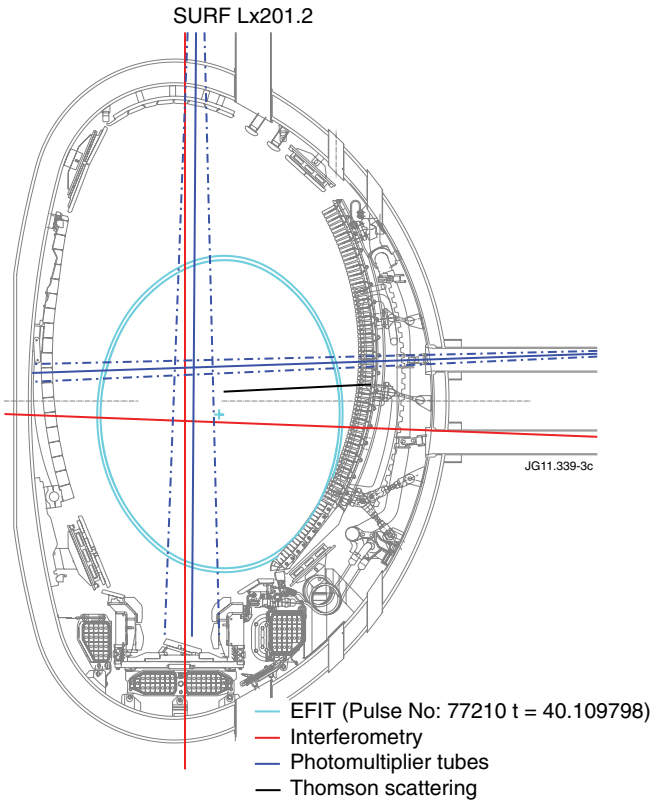


*Figure 2: (a) cyan circle : The outermost flux surface obtained with EFIT 109[ms] after plasma initiation, (b) red lines: line of sight for interferometry, (c) blue lines: line of sight for photomultiplier tubes, (d) black line : line of sight for Thomson scattering data.*

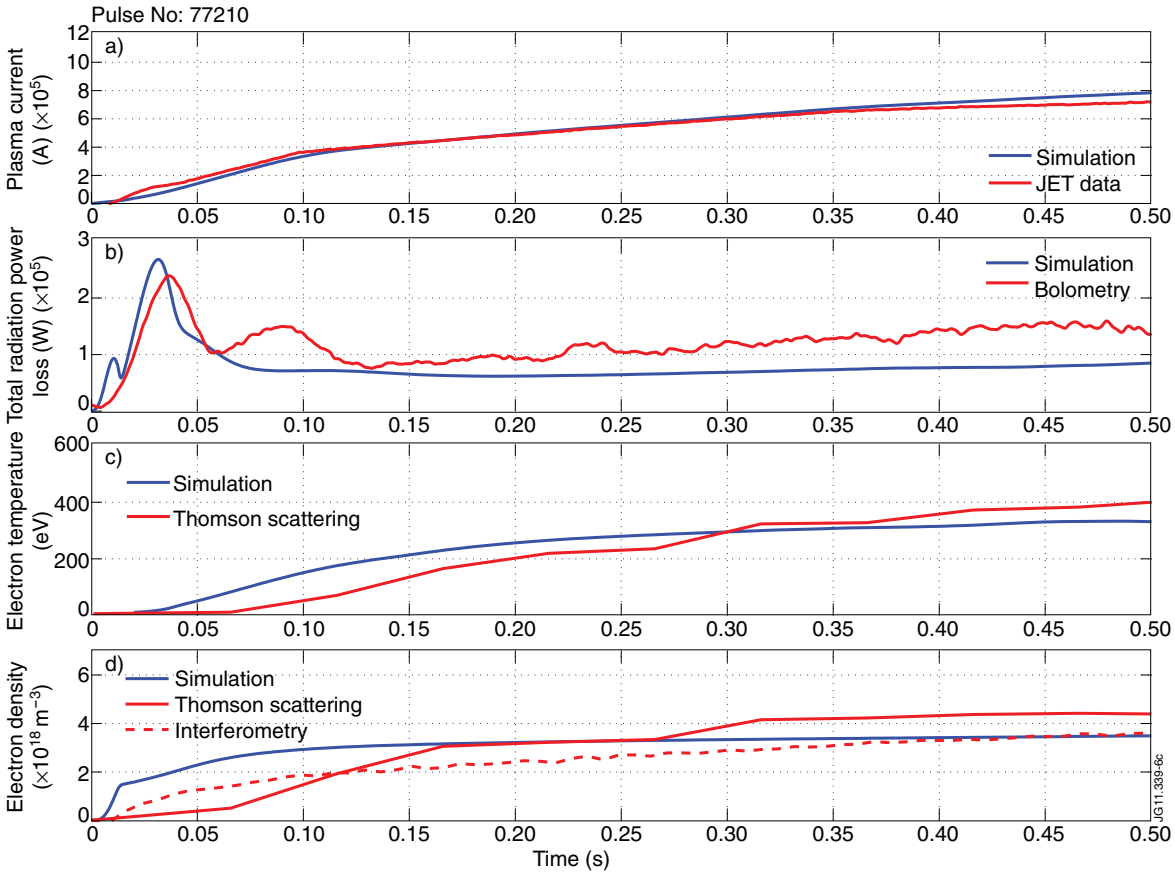


*Figure 3: Each figure show simulational results and JET data of (a) Plasma current, (b) Total radiation power (c) Plasma temperature and (d) plasma density. In all figures, red lines indicate JET data and blue lines describe the simulational results. The red dotted line in (d) represent electron density measured by interferometry.*

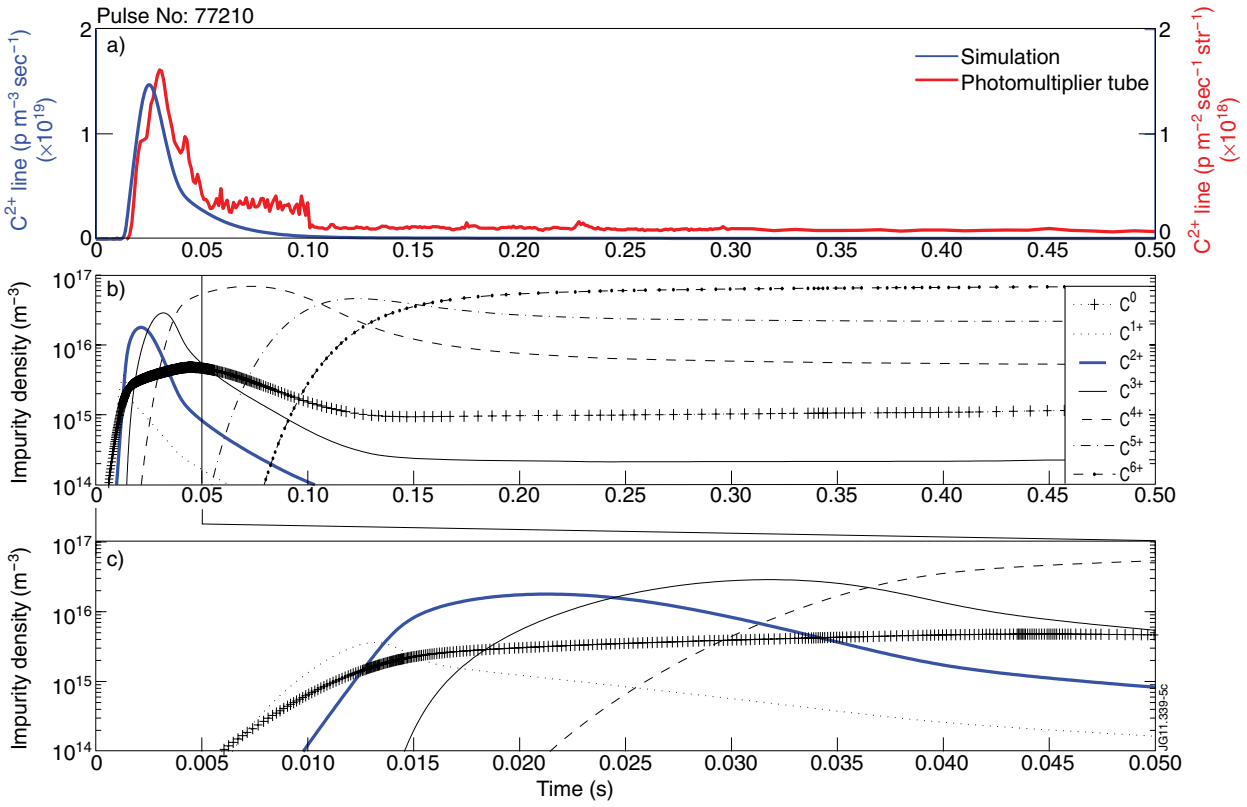


*Figure 4: The blue line in (a) indicates the synthetic data of $C^{2+}$ line(465[nm]) emission. The red lines in (a) shows $C^{2+}$ line(465[nm]) emission measured with the photomultiplier tube in JET. The different units in the simulated data ([p $m^{-3}sec^{-1}$]) and the measured data([p $m^{-2}$ $sec^{-1}str^{-1}$]) are indicated in the left and right y-axis, respectively. The change of $C^{2+}$ line in the simulation result and the measured data show good agreement, thereby implying reasonable impurity evolution. (b) shows the simulational evolution of carbon, and (c) represents the enlarged figure between 0 and 0.05 second in (b).*